Neurobiology of Disease

Altered Information Processing in the Prefrontal Cortex of Huntington's Disease Mouse Models

Adam G. Walker,[1,2] Benjamin R. Miller,[1,2] Jenna N. Fritsch,[1,2] Scott J. Barton,[1,2] and George V. Rebec[1,2]
[1]Program in Neuroscience and [2]Department of Psychological and Brain Sciences, Indiana University, Bloomington, Indiana 47405

Understanding cortical information processing in Huntington's disease (HD), a genetic neurological disorder characterized by prominent motor and cognitive abnormalities, is key to understanding the mechanisms underlying the HD behavioral phenotype. We recorded extracellular spike activity in two symptomatic, freely behaving mouse models: R6/2 transgenics, which are based on a CBA × C57BL/6 background and show robust behavioral symptoms, and HD knock-in (KI) mice, which have a 129sv background and express relatively mild behavioral signs. We focused on prefrontal cortex and assessed firing patterns of individually recorded neurons as well as the amount of synchrony between simultaneously recorded neuronal pairs. At the single-unit level, spike trains in R6/2 transgenics were less variable and had a faster rate than their corresponding wild-type (WT) littermates but showed significantly less bursting. In contrast, KI and WT firing patterns were closely matched. An assessment of both WTs revealed that the R6/2 and KI difference could not be explained by a difference in WT electrophysiology. Thus, the altered pattern of individual spike trains in R6/2 mice appears to parallel their aggressive form of symptom expression. Both WT lines, however, showed a high proportion of synchrony between neuronal pairs (>85%) that was significantly attenuated in both corresponding HD models (decreases of ~20% and ~30% in R6/2s and knock-ins, respectively). The loss of spike synchrony, regardless of symptom severity, suggests a population-level deficit in cortical information processing that underlies HD progression.

Key words: **bursting; spike synchrony; electrophysiology; transgenic; knock-in; corticostriatal pathway**

Introduction

Huntington's disease (HD) is an autosomal dominant disorder caused by an unstable polymorphic repeat of the CAG trinucleotide (The Huntington's Disease Collaborative Research Group, 1993). Patients with HD experience prominent motor symptoms such as chorea, dystonia, and bradykinesia as well as cognitive and psychiatric disturbances (Lawrence et al., 1996). Although the pathological hallmark of HD is degeneration of striatum and other basal ganglia structures (Vonsattel et al., 1985), morphological and functional changes in cerebral cortex may be fundamental to HD onset and progression (Lange et al., 1976; Sotrel et al., 1993; Paulsen et al., 2004; Feigin et al., 2006; Thiruvady et al., 2007). In fact, research on genetic mouse models indicates that an HD phenotype is expressed only when cortical pathology is detectable (Laforet et al., 2001).

In vitro electrophysiological studies have identified complex changes to ion channels and receptors that may ultimately render cortical neurons hyperexcitable (for review, see Cepeda et al., 2007). Metabolic mapping (Cybulska-Klosowicz et al., 2004; Mazarakis et al., 2005) and slice preparation studies (Cummings et al., 2006, 2007) have shown that cortical plasticity is also impaired in HD mice. Despite evidence implicating cortical dysfunction in HD, there is no information on real-time cortical operations in a behaving HD system, which is fundamental to understanding the HD behavioral phenotype. Thus, we recorded cortical neuronal activity in two symptomatic mouse models: R6/2 transgenics, which express a robust set of motor and cognitive symptoms (Mangiarini et al., 1996; Carter et al., 1999; Lione et al., 1999; Murphy et al., 2000), and an HD knock-in (KI) line, which shows a relatively mild symptom profile (Menalled et al., 2003; Dorner et al., 2007).

We assessed several aspects of cortical information processing. At the level of individual neurons, we monitored spike rate, as an index of overall activation, and burst activity, which can include spike clusters of varying rates and duration. Bursts are especially important for information transmission and synaptic plasticity (Lisman, 1997; Izhikevich et al., 2003), both of which are likely to be impaired in HD (Cepeda et al., 2007). We also assessed interactions between pairs of neurons by monitoring spike synchrony (Perkel et al., 1967; Gerstein, 1999), a property of neuronal populations (Sakurai, 1999). In fact, neuronal synchrony is a dynamic event correlated with behavioral output (Sakurai and Takahashi, 2006) and is likely to be disrupted in HD. Because striatal neurons are driven primarily by glutamatergic cortical input (Kemp and Powell, 1971; Fonnum et al., 1981), a detailed assessment of cortical activity may explain the abnormally high spike rate previously reported for R6/2 striatal neurons (Rebec et al., 2006). We focused on the prefrontal cortex

Received June 18, 2008; accepted July 23, 2008.

This work was supported by the National Institute of Neurological Disorders and Stroke Grant R01 NS35663 (G.V.R.). We thank Faye Caylor for administrative and editorial assistance; Paul Langley for technical support; and Tom Gaither, Alana Gilman, and Alexander Murphy-Nakhnikian for assistance with data collection.

Correspondence should be addressed to George V. Rebec, Program in Neuroscience and Department of Psychological and Brain Sciences, Indiana University, 1101 East 10th Street, Bloomington, IN 47405. E-mail: rebec@indiana.edu.

DOI:10.1523/JNEUROSCI.2804-08.2008

 0270-6474/08/288973-10$15.00/0

(PFC) because of its involvement in cognition (Dalley et al., 2004), its substantial striatal projections (Sesack et al., 1989; Vertes, 2004), and neuropsychological evidence implicating its dysfunction in HD patients (for review, see Lawrence et al., 1998).

Materials and Methods

Animals. Data were obtained from two genetically engineered mouse models of HD and their respective wild-type (WT) littermates. Male R6/2 transgenic (B6CBA-Tg [HDexon1] 62Gpb/1J) and WT littermates (CBA × C57BL/6) were obtained from The Jackson Laboratory between 5 and 6 weeks of age. After arrival, the mice were individually housed for the duration of the study. To confirm genotypes, tail samples of R6/2 and WT littermates were taken before perfusion (~12 weeks of age). A total of 11 R6/2 and 13 WT were used for this study.

Homozygous KI mice were bred in our colony from heterozygous breeding pairs obtained from an established colony at the University of California, Los Angeles (Menalled et al., 2003). Mice were weaned at 3 weeks of age, separated by sex, and housed with littermates. At ~8 weeks of age, tail samples for genotyping were obtained, and mice were transferred to individual housing for the duration of the study. A total of 18 KI male ($n = 8$) and female ($n = 10$) mice were used along with 13 male ($n = 7$) and female ($n = 6$) WT littermate (129sv) controls. KI and WT mice used in this spanned 20 different litters that were born over a 5.5 month time period.

All mice were housed in the departmental animal colony with *ad libitum* access to food and water and maintained on a 12 h light/dark cycle (lights on at 7:00 A.M.). All experimental procedures took place during the light cycle and were in accordance with the National Institutes of Health *Guide for the Care and Use of Laboratory Animals* and were approved by the Institutional Animal Care and Use Committee.

Genotype and CAG repeat length. Genomic DNA was extracted from tail tissue samples in 25 μl of cell lysis buffer (50 mM Tris, pH 8.0, 25 mM EDTA, 100 mM NaCl, 0.5% IGEPAL CA-630, and 0.5% Tween 20) and proteinase K (10 mg/ml; 60 μg/reaction) at 55°C for 2 h with gentle mixing after the first hour. DNA was diluted with 400 μl of filter-sterilized HPLC water, heated to 100°C for 10 min, centrifuged for 2 min at 17,000 × *g*, and stored at 4°C. PCR and analytical agarose gel electrophoresis were used to determine CAG repeat length. Primers were 31329 (5′-ATGAAGGCCTTCGAGTCCCTCAAGTCCTTC-3′) and 33934 (5′-GGCGGCTGAGGAAGCTGAGGA-3′) (Mangiarini et al., 1996). Each reaction consisted of 2.0 μl of DNA template (40–100 ng/μl), 0.4 μl of each primer (20 μM), 7.2 μl of filter-sterilized HPLC water, and 10.0 μl of 2× Biomix Red (Bioline USA) for 20 μl of total volume. Cycling conditions were 94°C for 90 s followed by 30 cycles of 94°C for 30 s, 62°C for 45 s, and 72°C for 90 s with a final elongation at 72°C for 10 min. Electrophoresis of samples was performed in 3.0% NuSieve 3:1 analytical agarose (Lonza Rockland) with 0.2 μg/ml ethidium bromide at 5 V/cm for 180 min using a 100 bp ladder as DNA standard.

Gels were evaluated with Kodak Image Station 4000R and Kodak Molecular Imaging software (Carestream Molecular Imaging) to confirm genotype and determine CAG repeat length. Using Clone Manager software (Sci-Ed Software), primers were aligned to the huntingtin gene sequence acquired from the National Center for Biotechnology Information (www.ncbi.nlm.nih.gov). Alignment of primers to template indicated that the DNA fragment amplified by PCR is 86 bp longer than the CAG repeat region. Computer analysis of fragment migration against the 100 bp standard showed that our R6/2 mice ($n = 16$) had 111.3 ± 1.6 (mean ± SEM) repeated CAG codons. Our KI mice ($n = 11$) had 125.3 ± 2.3 CAG codons.

Surgery. All mice were prepared for electrophysiological recording at the approximate time of symptom onset in the HD models. Surgery was performed on the R6/2 line and its corresponding WT at ~6.5–7 weeks of age and on the KI line and its corresponding WT at ~15 weeks of age. All mice were anesthetized with chloropent (0.4 ml/100 g) and placed in a stereotaxic apparatus. The scalp was shaved and prepared with betadine solution. Lidocaine (0.1 ml) was injected subcutaneously at the surgical site, and an incision was made at the midline to expose the skull. Holes were drilled bilaterally over PFC 1.5 mm anterior and 0.5 mm lateral relative to bregma. Microwire bundles constructed of three 25 μm Formvar-insulated recording stainless-steel wires and one 50 μm uninsulated stainless-steel ground wire were lowered into the brain 1.4 mm from the surface of the cortex, targeting the anterior cingulate (Cg1) and prelimbic (PrL) regions of the PFC. These regions are associated with various cognitive functions in rodents (Dalley et al., 2004) and densely innervate the striatum (Sesack et al., 1989; Vertes, 2004).

Bundles were attached to a custom plastic hub (6.0 mm diameter) via gold pins. The electrode assembly was chronically attached to the skull with screws and dental acrylic. Antibiotic cream was applied to the surgical site, and lactated Ringer's solution (1.0 ml) was injected subcutaneously to compensate for blood loss and prevent dehydration. All mice were allowed to recover from surgery for at least 7 d before electrophysiological recording. Animals were regularly monitored for signs of pain or complications during the recovery period.

Electrophysiology. After recovery, recording sessions routinely occurred once per week and ended for the R6/2-WT group when the animals reached ~12 weeks of age and for the KI-WT group at ~30 weeks of age. These ages encompass behaviorally symptomatic periods (Mangiarini et al., 1996; Rebec et al., 2002, 2003; Menalled, 2005; Dorner et al., 2007) without including the period of severe weight loss and disability that develops before death in the R6/2 model (Carter et al., 1999). During recording, the electrode assembly was connected to a light-weight, flexible wire harness, which was equipped with six field-effect transistors that provided unity-gain amplification to individual microwires. The harness was connected to a swiveling commutator that allowed the mouse freedom of movement throughout the recording session. Each recording session took place in an open-field environment inside a sound-attenuating chamber [61 cm length (L) × 51 cm width (W) × 71 cm height (H)]. The home cage (17 cm W × 27.5 cm L × 12 cm H) of each individual mouse with the lid removed served as the open field. Each recording session lasted 1 h, during which informal observations confirmed that the animals were behaviorally active.

Neuronal discharges were acquired by the Multichannel Acquisition Processor (MAP) system through a preamplifier (Plexon). The MAP system allows for direct computer control of signal amplification, frequency filtering, discrimination, and storage. To detect spiking activity, signals were bandpass filtered (154 Hz to 8.8 kHz) and digitized at a rate of 40 kHz. All spike sorting occurred online before the beginning of the recording session (Sort Client software from Plexon). After establishing a voltage threshold ≥2.5 times background noise, we collected a large number of waveform samples (~100–1000) and used principal component analysis to discriminate neurons. An oscilloscope and audio monitor were used to confirm that recorded signals were free of noise and that individual units were well isolated. Autocorrelograms and interspike interval (ISI) histograms were inspected to confirm the isolation of each unit. Collectively, these procedures indicated that template drift during a recording session was minimal; no off-line sorting was necessary.

All mice participated in multiple recording sessions, and units were often recorded on the same wire as a previous session. Day-to-day similarities in spike waveform and firing characteristics do not assure that the same neuron is being recorded, because slight electrode drift and subtle changes in behavioral state cannot be ruled out (Lewicki, 1998). Thus, units recorded on different days were treated as different units.

Behavioral characterization. Because HD affects diurnal cycles of behavioral activity (Morton et al., 2005), it is conceivable that any electrophysiological differences between HD and WT mice could be explained simply by differences in behavioral activity levels. Thus, we assessed videotapes made during our electrophysiological recording sessions on a subset of R6/2, KI, and respective WT mice ($n = 4$ per group). Ages for mice from the KI line assessed ranged from 17 to 30 weeks (mean = 22.6; SEM = 0.72). Mice assessed from the R6/2 line were 7–10 weeks of age (mean = 8.25; SEM = 0.13). We monitored the amount of time engaged in exploratory behavior, which included bouts of locomotion, digging, and sniffing, over a 30 min period. We also quantified time spent grooming and resting.

Histology. The brains of all mice were harvested to verify electrode placement. Animals received an overdose of chloropent (2.0 times the

surgical dose), and a small current (30 μA) was passed through individual wires (~10 s) to mark recording sites. Mice were then transcardially perfused with saline followed by 10% potassium ferrocyanide in 10% formalin. Brains were removed and cryoprotected in 30% sucrose in 10% formalin. They were frozen, cut into 50–60 μm sections on a sliding microtome, and mounted on gelatin-subbed slides for subsequent staining with cresyl violet and examination under a light microscope. Locations of lesions were compared with a stereotaxic atlas to determine placement of electrodes (Paxinos and Franklin, 2001).

Data analysis. Cortical neurons can be classified by firing rate and waveform into faster-spiking [>10 spikes/s with narrow afterhyperpolarizations (AHPs)] and slower-spiking (<10 spikes/s with wide AHPs) units (McCormick et al., 1985; Connors and Gutnick, 1990; Jung et al., 1998; Homayoun et al., 2005; Homayoun and Moghaddam, 2007), which are thought to correspond to interneurons and pyramidal cells, respectively (McCormick et al., 1985; Connors and Gutnick, 1990; Homayoun and Moghaddam, 2007). To determine whether neurons with a firing rate >10 spikes/s represented a separate class of neurons, the average of 50 waveforms from each faster-spiking neuron was plotted, and the AHPs were measured. These data were compared with a random sample of AHPs from those classified as slower-spiking cells based on firing rate.

Time stamps from neuronal data were analyzed with NeuroExplorer software (NEX Technologies). To characterize the spontaneous activity of neurons in PFC, we analyzed overall firing rates, variability, and bursting as well as spike synchrony. Firing rates were calculated by dividing the total number of spikes by the length of the entire recording session. Spike-train variability was assessed by calculating the coefficient of variation (CV) of the ISI for each individual spike train. CV ISI was calculated by dividing the SD of the ISI by the mean ISI in the spike train across the entire recording session (Young et al., 1988). A larger CV ISI value indicates more variability and thus a more irregularly firing neuron (Homayoun et al., 2005).

We used the burst surprise algorithm to detect and quantify bursting activity of spike trains. This algorithm uses a probability-based approach to burst detection that compares successive ISIs in a spike train to a Poisson spike train with the same firing rate. If a set of consecutive ISIs occurs with a sufficiently low probability, the event is considered "surprising" and classified as a burst. The algorithm requires the investigator to set a minimum surprise value that must be exceeded for an event to be classified as a burst (Legéndy and Salcman, 1985). We used a value of 5 as our minimum surprise, which corresponds to the burst occurring ~150 times more frequently ($p < 0.007$) than in a Poisson distribution with the same firing rate (Homayoun et al., 2005). Bursting properties that we analyzed included burst rate, percentage of all spikes that occurred in bursts, mean burst surprise, mean burst duration, mean ISI in a burst, mean burst frequency, and mean number of spikes per burst.

Synchrony was analyzed by constructing cross-correlation histograms (±500 ms, 1 ms bin width) between simultaneously recorded units (Perkel et al., 1967). A pair of neurons was considered synchronous if there was a clear peak that exceeded the 99% confidence limit as described previously (Abeles, 1982). Because we were interested in how local populations of neurons process information, we only analyzed synchrony between neurons that were recorded ipsilaterally. Furthermore, because we cannot detect simultaneous spikes recorded from pairs of neurons on the same wire, neuronal pairs recorded from the same wire were excluded from synchrony analysis. Also note that we view synchrony in terms of simple coactivation of pairs of neurons and make no assumptions about anatomical connectivity (Hampson and Deadwyler, 1999).

Statistical analysis. All statistical analyses were made using GraphPad Prism (GraphPad Software). Open-field behaviors were compared using a two-way ANOVA (group × behavior). Nonparametric Mann–Whitney *U* tests were used to compare AHP of fast-spiking and regular-spiking cells as well as firing rates, bursting, and spike-train variability data between the HD and WT mice in both lines. Nonparametric statistical approaches were preferred because of the significant deviation from normality and a lack of homogeneous variances that existed in our spike data (Zar, 1999). Pearson's χ^2 test was used to determine differences in the proportions of synchronous neurons between HD and corresponding WT animals.

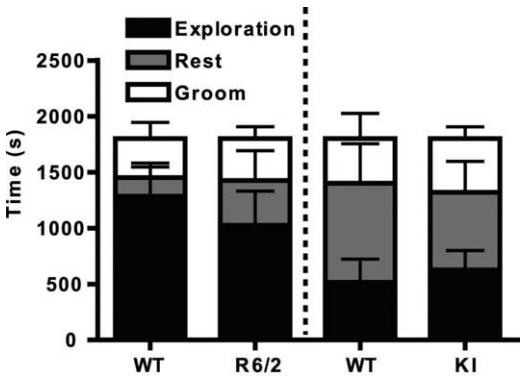

Figure 1. Characterization of open-field behavior for all groups of mice. Behavior was classified as exploration (black), resting (gray), or grooming (white). Overall behavioral activation was comparable across groups, because there was no significant group main effect. Each bar represents the mean time spent engaged in the behavior indicated, and the error bars indicate SEM.

Results

All mice were behaviorally active for the duration of all recording sessions. Exploratory activity (locomotion, sniffing, and occasional digging) predominated between brief bouts of grooming and resting. This general behavioral pattern appeared in both HD lines and their respective WTs; there was not a significant group main effect in the amount of time engaged in exploration, grooming, or resting (Fig. 1) ($p > 0.05$), making it unlikely that the level of behavioral activity alone could explain any group neuronal differences. As expected, however, HD mice were symptomatic, showing hindlimb flicks, tremor, and motor slowness, as reported previously (Mangiarini et al., 1996; Carter et al., 1999; Rebec et al., 2002, 2003; Dorner et al., 2007). These symptoms were more pronounced in R6/2 mice, consistent with the more aggressive form of HD that appears in this line (Carter et al., 1999). Also consistent with previous data on inbred mouse strains (Holmes et al., 2002), the R6/2 WT (CBA × C57BL/6) (Mangiarini et al., 1996) showed a more varied behavioral repertoire (digging, rearing, running, and walking) than the KI WT (129sv) (Menalled et al., 2003).

Neuron characteristics

We recorded a total of 489 neurons: 186 from the transgenic (R6/2, $n = 90$; WT, $n = 96$) and 303 from the KI (KI, $n = 162$; WT, $n = 141$) lines. Histological analysis confirmed that all electrode placements were in Cg1 and PrL; most electrodes were placed between 2.6 and 1.8 mm anterior to bregma (Fig. 2*A*). Data obtained from electrodes placed in Cg1 were compared with those from electrodes in PrL, and it was determined that there were no differences between the regions. Because we used both sexes of the KI line, we analyzed their neuronal data for evidence of a sex difference, but found none. Thus, KI data include males and females in both KI and WT groups.

Cortical neurons can be classified by firing rate and waveform as either faster-spiking (>10 spikes/s) units with narrow AHPs or slower-spiking (<10 spikes/s) units with relatively wide AHPs (McCormick et al., 1985; Connors and Gutnick, 1990; Homayoun and Moghaddam, 2007). Our firing rate analysis revealed a total of 49 faster-spiking units, accounting for ~10% of the total (49 of 486) and distributed relatively evenly across each of our four groups of mice. An average of 50 waveforms from each

fast-spiking unit were plotted, measured, and compared with a random sample of AHPs from slower-spiking units. We found no difference in AHPs ($p > 0.05$), and thus did not distinguish between fast- and slow-spiking units in all subsequent analyses. Thus, all recorded neurons appear to represent a homogeneous population, most likely pyramidal cells (McCormick et al., 1985; Connors and Gutnick, 1990; Homayoun and Moghaddam, 2007). Representative waveforms are displayed in Figure 2*B*.

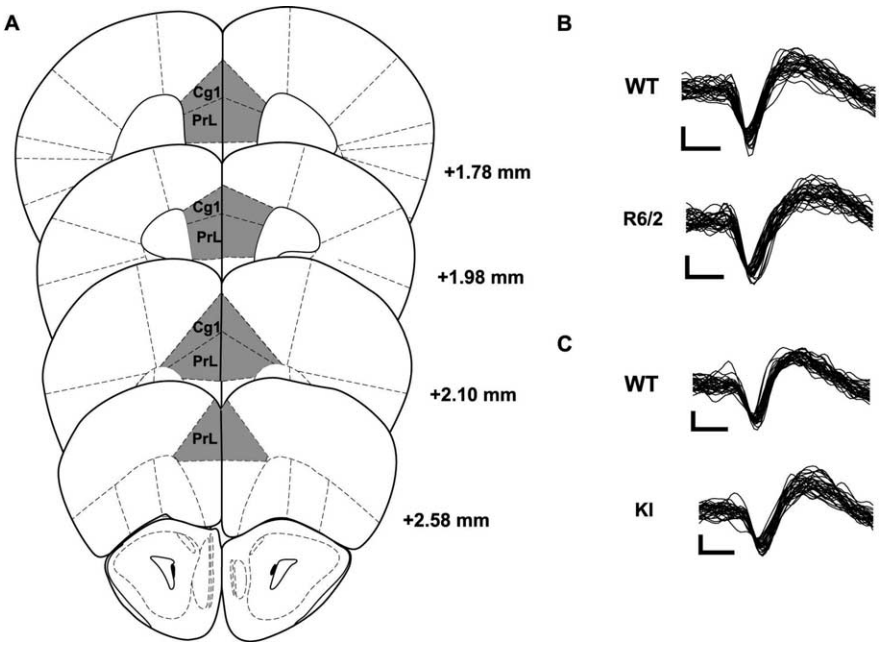

Figure 2. ***A***, All microwire bundles were placed within the Cg1 and PrL subregions of the PFC. ***B***, ***C***, Representative waveforms from putative pyramidal neurons recorded in WT and R6/2 mice (***B***) and WT and KI mice (***C***). There were no significant group differences between waveform shape and size. Calibration: 25 μV, 250 μs.

Background strain comparisons

We first tested for influence of genetic background by comparing the respective WTs: CBA × C57BL/6 hybrid in the case of the R6/2 line (Mangiarini et al., 1996) and the 129sv strain in the case of the KI line (Menalled et al., 2003). Generally, C57BL/6 mice tend to perform better on learning and memory tasks and show more robust synaptic plasticity in the hippocampus than most other strains, including CBA and 129sv (Crawley et al., 1997; Holmes et al., 2002; Nguyen, 2006). The 129sv mice also exhibit less exploratory and locomotor behavior than C57BL/6J mice (for review, see Holmes et al., 2002). Figure 3, *A* and *B*, shows that the 129sv had a faster spontaneous firing rate and greater burst rate than the CBA × C57BL/6 ($p < 0.01$). Bursting appears to occur differently in each strain, because some aspects of burst structure were also different (Table 1). Burst duration and the ISI within a burst, for example, were both greater in the CBA × C57BL/6 ($p < 0.001$), whereas 129sv mice had a faster firing rate within a burst ($p < 0.001$). Importantly, there was no significant difference between spike train variability, number of spikes per burst, the percentage of spikes occurring in bursts, or the burst surprise value ($p > 0.05$). Also, both WTs had comparable levels of spike synchrony: 89% in CBA × C57BL/6 and 93% in 129sv ($\chi^2 = 0.759$; $p > 0.05$). Thus, although aspects of information processing may be different in each strain, bursting and spike synchrony are prominent features of PFC neurons regardless.

Firing rate and spike-train variability in HD

Spontaneous firing rates during a recording session for all units in all groups of HD and WT mice are shown in Figure 4. A significant increase in rate relative to WT emerged in R6/2 ($p < 0.01$) but not KI mice. A similar outcome characterized our assessment of spike-train variability: R6/2 ($p < 0.01$) but not KI mice had a significantly lower CV compared with their respective WT (Table 1). Thus, only R6/2s show a faster overall rate and a less variable pattern of firing than WT.

Burst activity in HD

R6/2 mice also differed from WT littermates in burst activity. As shown in Figure 5*A–C*, WT mice displayed significantly more bursting ($p < 0.05$), a greater percentage of spikes participating in bursts ($p < 0.001$), and a higher burst surprise value ($p < 0.05$) than R6/2s. It appears, therefore, that bursts are a common property of cortical activity in WT controls, whereas R6/2 mice rely on a relatively regular pattern of individual spikes. Interestingly, however, when a burst occurred in R6/2 mice, it was not structurally different from a WT burst. Table 1, for example, shows no significant WT and R6/2 differences related to burst duration or to within-burst events such as spike frequency, number of spikes, and ISI. In contrast, no aspect of burst activity differed from WT controls in the KI line. Figure 5*D–F* shows virtually identical burst activity in these groups. Similarly, the structure of individual bursts was not different (Table 1).

Key features of spike-train activity are shown in representative 10 s raster plots recorded from individual mice (Fig. 6*A*,*B*). For the transgenic comparison (Fig. 6*A*), burst activity, highlighted in gray, is a prominent feature of WT, but not R6/2, spiking. Also note that the R6/2 spike train contains more spikes, reflecting the increase in rate, and the ISIs appear less variable than WT. The WT and KI comparison (Fig. 6*B*), however, reveals remarkably similar burst and spike activity.

Synchrony in HD

To characterize synchronous activity among local populations of neurons, we constructed cross-correlation histograms whenever two or more units were recorded ipsilaterally. We excluded neurons recorded on the same microwire, because simultaneous spikes from such recordings cannot be distinguished. These restrictions allowed us to analyze 100 cross-correlation histograms in the transgenic (48 WT and 52 R6/2) and 140 cross-correlation histograms in the KI (91 WT and 49 KI) groups.

Pairs of PFC neurons recorded from WT controls for both R6/2s and KIs show a high degree of synchronous discharges as indicated by tall, sharp central peaks in individual cross-correlation histograms. Representative examples are shown in Figures 7*A* and 8*A*. A magnified view showing the 99% confidence limit (black dashed line) and expected mean (white dashed line) is presented in Figures 7*C* and 8*C*. Note in both cases that the central peak is well beyond the 99% confidence limit. Rasters shown in Figures 7*E* and 8*E* illustrate the high degree of temporally precise discharges evident in WT neuronal pairs. In fact,

Table 1. Spike train variability and burst structure for transgenic and knock-in mouse models of HD and corresponding WT littermates

	WT			R6/2 or KI		
	Median	Range	25th to 75th percentile	Median	Range	25th to 75th percentile
Transgenic model (R6/2)						
Variability						
CV ISI	1.338*	1.005–9.583	1.198–1.579	1.258	0.929–3.688	1.147–1.417
Burst structure						
Duration (s)	1.283†	0.191–14.07	0.759–2.288	1.006	0.166–34.90	0.062–2.128
Spikes/s	24.92†	2.579–160.3	14.71–43.39	31.85	1.473–114.8	16.90–49.64
Spikes/burst	15.67	5.00–60.38	12.56–20.81	16.27	6.00–87.40	13.00–21.38
ISI in a burst (s)	0.098†	0.012–0.996	0.049–0.137	0.068	0.012–0.927	0.036–0.126
Knock-in model (KI)						
Variability						
CV ISI	1.28	0.097–11.83	1.158–1.50	1.316	1.030–3.289	1.201–1.583
Burst structure						
Duration (s)	0.832	0.067–187.4	0.548–1.566	0.787	0.156–54.68	0.488–1.148
Spikes/s	40.95	0.176–123.5	25.21–58.77	38.91	0.463–180.0	21.38–58.79
Spikes/burst	15.59	4.80–48.63	12.54–19.82	15.15	7.054–36.11	12.67–19.84
ISI in a burst (s)	0.057	0.014–5.680	0.039–0.096	0.053	0.008–3.212	0.034–0.102

*$p < 0.01$, significant difference between medians of R6/2 and WT. †$p < 0.0001$, significant differences between medians of WT mice from the transgenic and WT mice of the KI line.

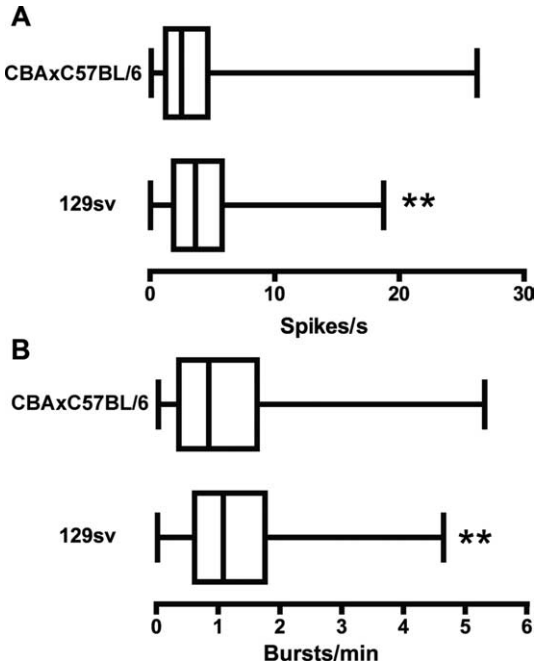

Figure 3. Comparison of WT littermate controls between the two mouse models of HD. Data in ***A*** and ***B*** are presented as box-and-whiskers plots. The left edge of the box is the 25th percentile, the center line is the median (50th percentile), and the right edge is the 75th percentile. The far left whisker extends to the lowest value in the distribution and the far right to the highest value. Asterisks indicate statistically significant differences between medians based on a Mann–Whitney *U* test. ***A***, WT mice from the KI line (129sv) had a significantly faster spontaneous firing rate than those from the R6/2 line (CBA × C57BL/6; $^{**}p < 0.01$). ***B***, 129sv mice had a significantly greater burst rate than CBA × C57BL/6 mice ($^{**}p < 0.01$).

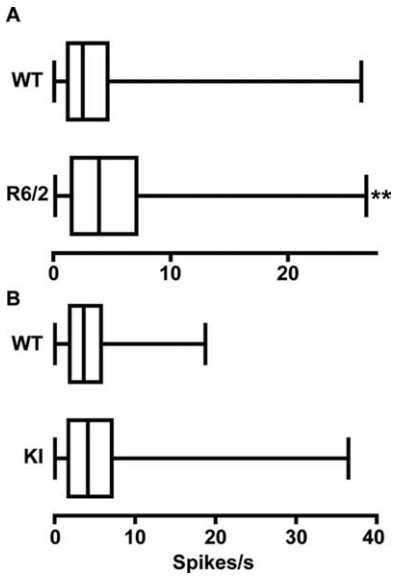

Figure 4. Spontaneous firing rates. ***A***, R6/2 mice had a significantly faster firing rate than WT mice ($^{**}p < 0.01$). ***B***, There were no significant differences between the firing rates in the KI and WT mice. Data are presented as in Figure 3.

89% of neuronal pairs were synchronous in WT mice from the R6/2 line, and 93% were in those from the KI model. Synchrony was much less common, however, in both lines of HD mice. Note the lack of a central peak for the R6/2 and KI recordings shown in Figures 7, *B* and *D*, and 8, *B* and *D*, respectively, and the absence of temporal precision among neuronal pairs (Figs. 7*F*, 8*F*). Only 68 and 58% of neuronal pairs were synchronous in the R6/2 and KI models, respectively. Overall, a significantly greater proportion of synchronous discharges were detected in the WTs compared with their respective R6/2 ($\chi^2 = 8.23$; $p < 0.01$) and KI ($\chi^2 = 26.91$; $p < 0.01$) littermates. Notably, there was not a significant difference in synchrony between the R6/2 and KI mice ($\chi^2 = 1.60$; $p > 0.05$). The decline in spike synchrony in both HD lines indicates impaired processing of information by PFC neuronal populations.

Electrophysiological changes in early- versus late-symptomatic R6/2 mice

Unlike KI mice, which show a relatively stable behavioral phenotype across the age ranges tested here (Menalled et al., 2003; Dorner et al., 2007), R6/2s show a more dynamic pattern characterized by relatively mild symptoms at ~8 weeks of age that become severe several weeks later (Carter et al., 1999; Lione et al., 1999). Thus, we evaluated R6/2 electrophysiological data collected during early (7–9 weeks; $n = 33$ units) and late (10–12 weeks; $n = 57$ units) symptomatic stages. Figure 9*A* shows that there was no significant difference in firing rate of neurons recorded from 7- to 9-week-old and 10- to 12-week-old R6/2s ($p > 0.05$), and there was no difference in spike-train variability ($p > 0.05$). Burst

activity also was equivalent in both age groups, as demonstrated by burst rate (Fig. 9*B*) ($p > 0.05$), percentage of spikes occurring in bursts (Fig. 9*C*) ($p > 0.05$), and burst surprise values (Fig. 9*D*) ($p > 0.05$). Synchrony also was comparable across age ($\chi^2 = 0.167$; $p > 0.05$): 73% of neuronal pairs were synchronous in early- and 67% in late-symptomatic mice. Thus, changes in cortical activity in R6/2 mice are evident early and persist throughout the disease process.

Discussion

Our results indicate impaired information processing in PFC of behaviorally active, symptomatic HD mice. In fact, the impairment extends beyond the level of individual neurons to suggest a problem of communication between neurons. Thus, although changes occur at the single-unit level, they occur in R6/2s, which have an especially robust symptom profile, but not in KI mice, which express a relatively mild phenotype throughout. In both models, however, interneuronal processing is severely impaired as revealed by a reduction in spike synchrony. Thus, despite differences in behavior and genetic background, these models suggest a processing deficit in PFC neuronal populations as a key feature of HD.

Differences in PFC activity of background strains

KI WT mice (129sv) appear to have a greater firing and burst rate relative to those from the R6/2 line (CBA × C57BL/6). Differences in burst structure also exist between the WTs. This is not surprising given their differences in behavior and physiology (Crawley et al., 1997; Holmes et al., 2002; Nguyen, 2006). Other important properties, such as spike variability, percentage of spikes occurring in bursts, and burst surprise values, are not different. Therefore, the few differences in single-unit activity that exist in WTs cannot account for the complex alterations in individual neurons of R6/2 but not KI mice. Synchrony in both lines, moreover, is comparable with ~90% of neurons discharging synchronously.

Altered single-unit patterns in R6/2

The elevated firing rate we observe in R6/2s is consistent with *in vitro* studies indicating that cortical pyramidal neurons are hyperexcitable (for review, see Cepeda et al., 2007). Furthermore, increased cortical activity may explain the elevated discharge rate in striatum of R6/2s (Rebec et al., 2006) as striatal neurons receive massive excitatory input from cortex (Fonnum et al., 1981). Our findings are also

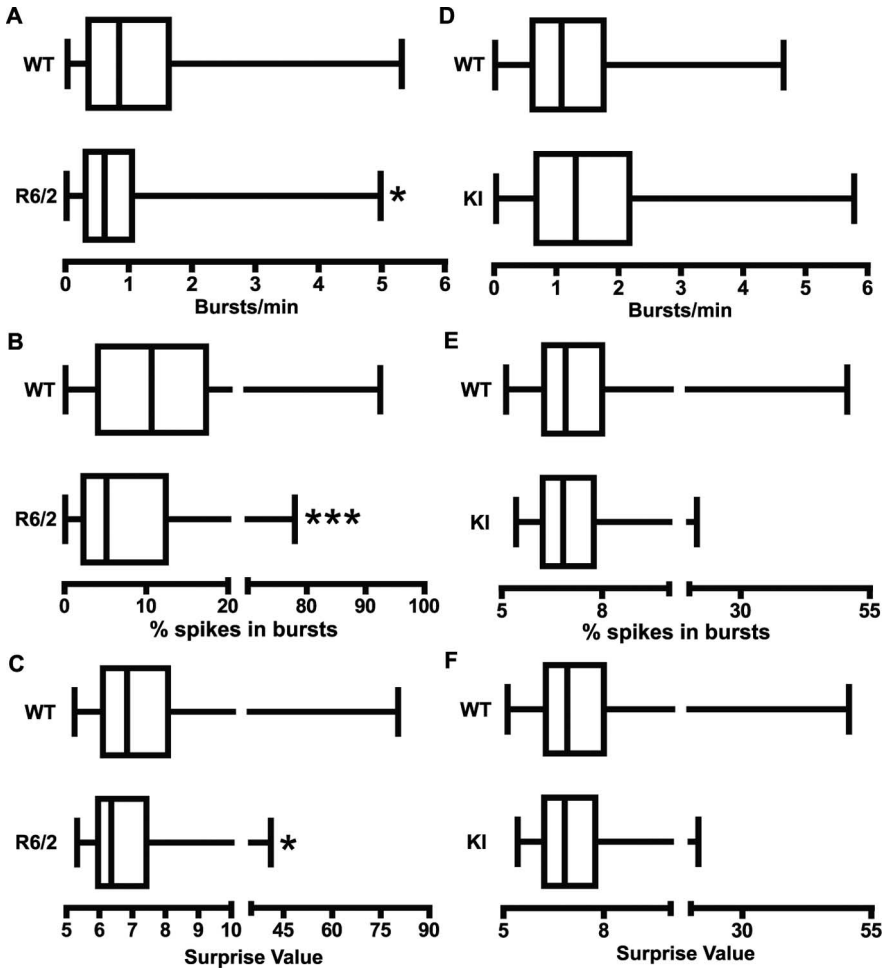

Figure 5. Bursting activity. ***A–C***, R6/2 mice had a significantly lower burst rate (***A***; $*p < 0.05$), percentage of spikes occurring in bursts (***B***; $***p < 0.001$), and burst surprise value (***C***; $*p < 0.05$) than WT. ***D–F***, There were no significant differences in bursting activity between WT and KI mice. Data are presented as in Figure 3.

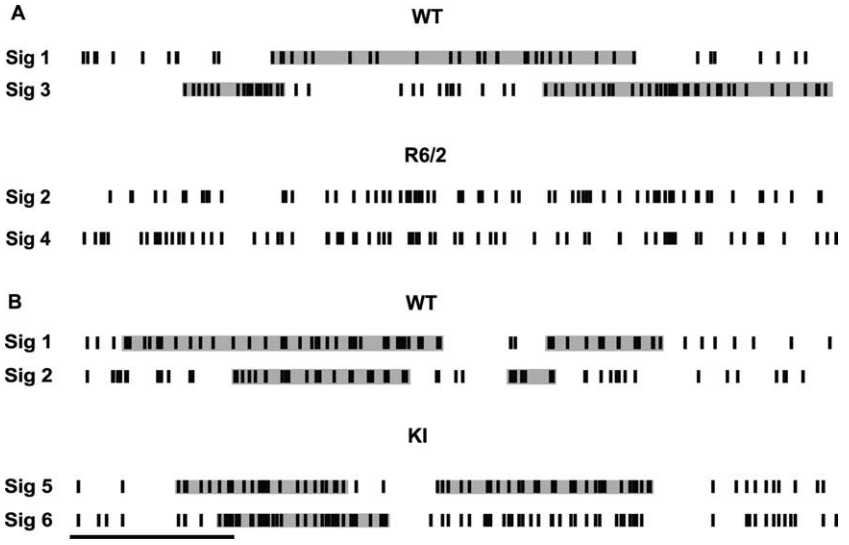

Figure 6. Example 10 s spike train rasters from all groups. ***A***, WT spike trains were characterized as having significant burst activity (highlighted in gray), which was significantly reduced in R6/2 mice. Note that there appear to be more spikes with less variable ISIs in the R6/2 raster relative to WT, indicative of the increased firing rate and reduced variability, respectively. ***B***, Characteristics of single spike trains did not differ significantly between WT and KI mice. Both contain significant burst activity and were similar in firing rate and variability. Sig refers to a signal recorded from a single unit. Calibration: 2 s.

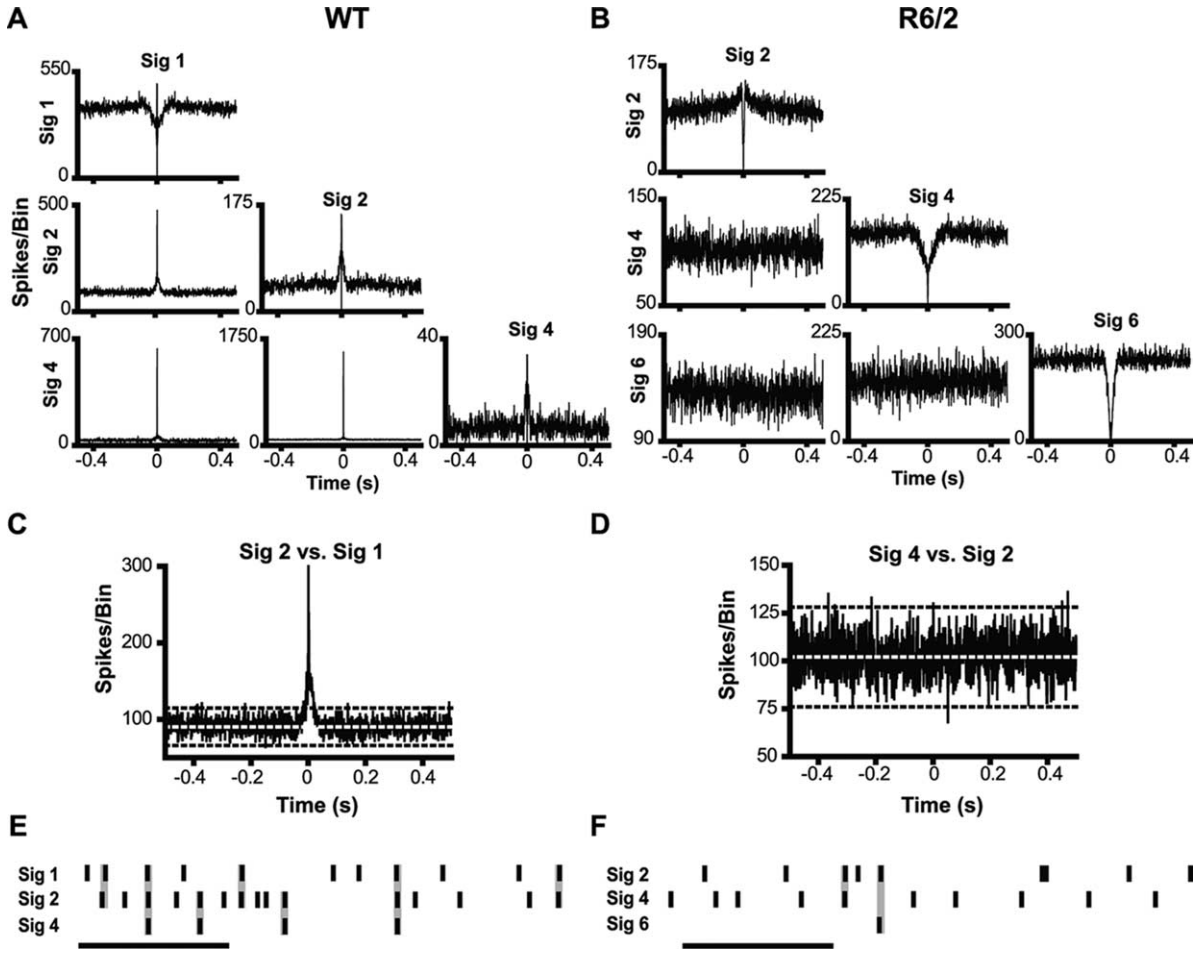

Figure 7. Spike synchrony in a transgenic mouse model of HD. ***A***, ***B***, Example cross-correlation histogram matrices generated from simultaneously recorded pairs of neurons in WT and R6/2 mice. Histograms along the diagonal are autocorrelogram functions for each of the units. The presence of a central trough and line that terminates near zero on the abscissa is indicative of a refractory period. ***A***, Neuronal pairs recorded in WT mice tended to have sharp central peaks, indicative of synchronous discharges. ***B***, These sharp peaks were often noticeably absent in R6/2 mice. ***C***, ***D***, Enlarged cross-correlation histograms from WT and R6/2 mice displaying the expected mean (white dotted line) and 99% confidence limit (black dashed line). ***E***, ***F***, Example 1 s rasters from WT and R6/2 mice. Calibration: 250 ms. At this time scale, it is apparent that synchronous spiking (highlighted in gray) occurs often in WT mice (***E***), but not in R6/2 mice (***F***). Sig refers to a signal recorded from a single unit.

consistent with human imaging studies demonstrating PFC hyperactivity in HD (Feigin et al., 2006).

Although burst structure in HD mice was not different from WT, significant decreases in burst rate and percentage of spikes occurring in bursts for R6/2s indicate that bursting is less prominent than in WT. Furthermore, when a burst occurs in R6/2s, it is less salient relative to background spiking, as indicated by decreased burst surprise (Legéndy and Salcman, 1985). Because bursting is important for synaptic plasticity and information encoding (Lisman, 1997; Izhikevich et al., 2003), decreased bursting in R6/2s is consistent with reports indicating compromised plasticity in HD cortex (Cybulska-Klosowicz et al., 2004; Mazarakis et al., 2005; Cummings et al., 2006, 2007; Crupi et al., 2008). Our data extend these findings by indicating compromised information encoding in R6/2 PFC neurons.

The changes in firing rate, spike-train variability, and bursting in R6/2s are nearly identical to changes seen in PFC of rats treated systemically with the NMDA antagonist (+)-5-methyl-10,11-dihydro-5*H*-dibenzo [a,d] cyclohepten-5,10-imine maleate (MK-801) (Jackson et al., 2004; Homayoun et al., 2005; Homayoun and Moghaddam, 2007). These two models also exhibit behavioral similarities. MK-801 administration, for example, results in an increase in behavioral stereotypies (Jackson et al., 2004). Behaviors in R6/2 mice are also highly stereotyped, such as the hindlimb flick (Carter et al., 1999) and decrease in spontaneous turning (Rebec et al., 2003). Evidence suggests that dysregulated firing patterns caused by MK-801 result from decreased activation of inhibitory interneurons, leading to pyramidal disinhibition (Homayoun and Moghaddam, 2007). Interestingly, decreased inhibition of pyramidal cells by interneurons also occurs in conditional KI HD mice (Gu et al., 2005). Metabotropic glutamate receptor 2/3 (mGluR2/3) agonists reverse the neural and behavioral effects of MK-801 (Homayoun et al., 2005). In R6/2 mice, mGluR2/3 autoreceptors, which inhibit glutamate release (Schoepp et al., 1999), are downregulated in cortex and striatum (Cha et al., 1998), and chronic treatment with mGluR2/3 agonists increases survival time and mildly improves some phenotypic behaviors (Schiefer et al., 2004). It is conceivable that the altered firing patterns observed in R6/2s result from the combination of decreased inhibition of glutamate release and reduced inhibition of pyramidal cells by interneurons. These mechanisms could contribute to the behavioral phenotype expressed in R6/2s (see also Cepeda et al., 2007). When combined with deficient glutamate uptake in the striatum (Liévens et al., 2001; Miller et al., 2008a), increased PFC activity could account for striatal hyperactivity in R6/2s (Rebec et al., 2006). Increased firing, moreover, leaves striatal neurons vulnerable to excitotoxicity, which is common in HD (DiFiglia, 1990).

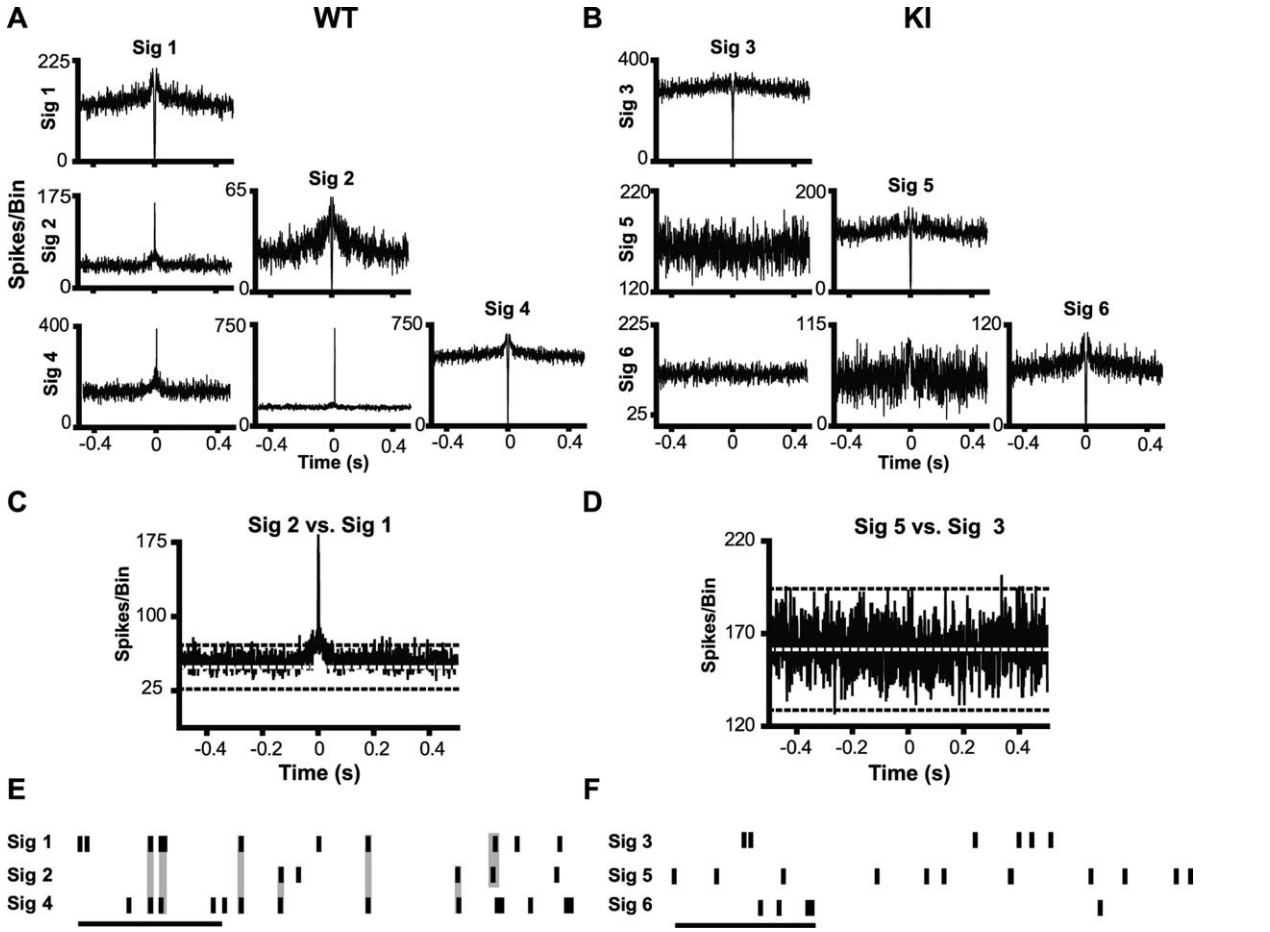

Figure 8. Spike synchrony in a KI mouse model of HD. ***A***, ***B***, Sharp peaks often occur in cross-correlation histograms constructed from WT neuronal pairs (***A***), but not KI (***B***). ***C***, ***D***, Examples of enlarged cross-correlation histograms from WT and KI mice with expected means and 99% confidence limit. ***E***, ***F***, Spike trains from WT mice contained a large number of synchronous spikes (***E***), which were noticeably absent from KI mice (***F***). Calibration: 250 ms. Sig refers to a signal recorded from a single unit.

Disruption of neuronal population activity in HD

Because synchrony was reduced in both R6/2 and KI mice, it may be a more reflective measure of the underlying cellular pathology in HD than firing rate or bursting. Thus, a loss of cortical synchrony is likely a robust feature of HD, despite differences in gene expression and phenotype between transgenic and KI models (Hickey and Chesselet, 2003). Synchrony is thought to represent information coding by neuronal populations that may be undetectable in single-unit activity (Sakurai, 1999). In monkeys, a high proportion of PFC neurons fire synchronously during a working memory task retention period, even when firing rate of single neurons does not change (Sakurai and Takahashi, 2006). Furthermore, Thiruvady et al. (2007) reported that activation between PFC subregions during a cognitive task is poorly correlated in HD. Thus, synchronous activation appears to be an important property of neuronal populations in the production of normal behavioral output.

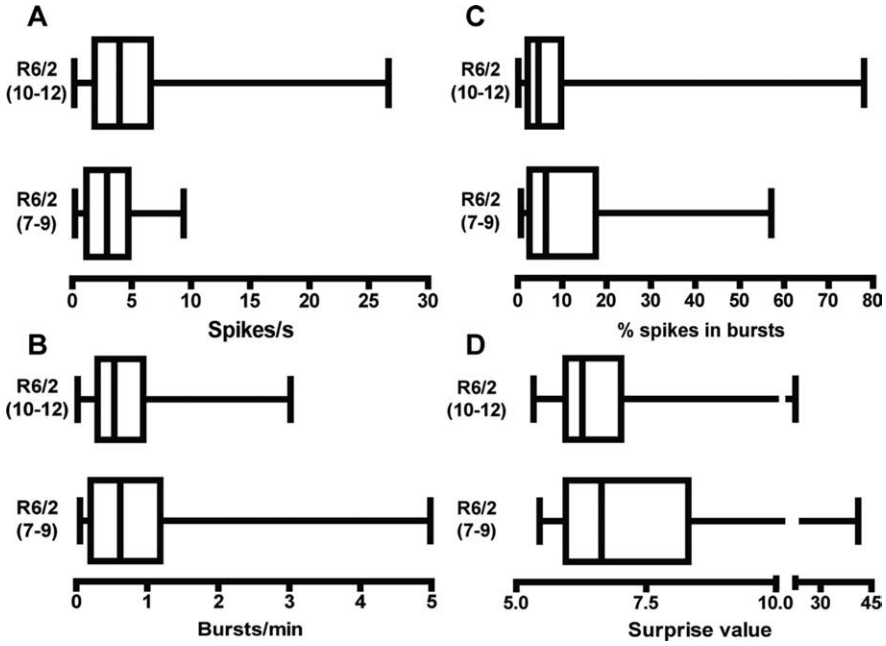

Figure 9. Comparison of electrophysiological data from 7- to 9-week-old and 10- to 12-week-old R6/2 mice. ***A–D***, There were no significant differences in firing rate (***A***) or burst activity (***B–D***) between the two groups. Data are presented as in Figure 3.

Although our results were obtained from putative pyramidal neurons, it would be interesting to assess activity of interneurons given their role in cortical synchrony (Hestrin and Galarreta, 2005) and evidence of disruption in HD (Gu et al., 2005). Our sample, however, does not appear to contain interneurons, which is not uncommon for *in vivo* cortical recordings (Contreras, 2004).

One could argue that reduced synchrony reflects differences in firing rate between HD and WT mice, but this is unlikely because the probability that spikes from one neuron would occur in close temporal proximity to spikes from another neuron (i.e., synchronously) increases with faster firing rates. In fact, although R6/2s have a faster firing rate than WT, there was a reduction in synchrony. Additionally, 129sv mice had an increased firing rate relative to CBA × C57BL/6, yet synchrony was not different. Our experimental methods, moreover, limit the possibility that differences in synchrony occur by chance. For one, recordings occurred while mice were freely behaving, and no stimuli were presented that could comodulate the firing rate of a pair of neurons to produce synchrony (Gerstein, 1999). Also, data were continuously recorded over a 1 h period, providing a large sample to construct cross-correlation histograms for an accurate reflection of population activity. Finally, our spike-sorting paradigm ensured that templates represented a single neuron and were free of noise. Thus, reduced synchrony is likely a real property of PFC neurons in HD.

The corticostriatal pathway and symptom severity

Preliminary data from recordings in behaving R6/2 and KI mice have revealed that striatal neurons exhibit decreased bursting and synchrony (Miller et al., 2008b). Because KI mice do not exhibit bursting changes in PFC, it is tempting to speculate that alterations occur in striatum before cortex in HD. One could also argue, however, that striatal neurons require coincident excitation from cortex or thalamus to bring them into a depolarized up-state for bursting to occur (Wilson and Kawaguchi, 1996). Reduced synchrony in cortex could lead to a lower probability of coincident excitation of striatal neurons, suggesting that reduced bursting in HD striatum (Miller et al., 2008b) may be a consequence of reduced cortical synchrony.

Our data also suggest that alterations of PFC activity are related to symptom severity. PFC information processing may be altered at the population level in HD when symptoms are relatively mild, as modeled by reductions in synchrony in KI mice. More severe forms of HD, represented by the R6/2 model, would be characterized by additional changes to individual neurons, such as rate, spike variability, or bursting. This relationship between symptom severity and PFC alterations is consistent with studies demonstrating that cortical changes are necessary for the development of the HD phenotype (Laforet et al., 2001). It is possible that KI neurons develop rate and burst changes at an older age, when behavioral abnormalities become more apparent (Menalled et al., 2003).

Conclusion

Electrophysiological analysis of PFC activity in behaving, symptomatic mouse models of HD and their corresponding WTs reveals information-processing deficits at both the single-neuron and population levels. In single neurons, the rate and pattern of firing appear to reflect symptom severity, because they are altered in R6/2 mice, known for their severe symptom profile, but not KI mice, which display a mild phenotype. Consistent with this view, well known behavioral differences between the CBA × C57BL/6 hybrid and the 129sv WTs were accompanied by single-unit differences in firing rate and pattern. Both WTs, however, showed similar amounts of synchronous activity between simultaneously recorded neurons, whereas synchrony was significantly reduced in both HD models. Thus, deficits in interneuronal communication are a common feature of the R6/2 and KI models despite differences in symptom profile and genetic background. It appears, therefore, that a population-level deficit in neuronal information processing in PFC is an underlying feature of the HD behavioral phenotype.

References

Abeles M (1982) Quantification, smoothing, and confidence limits for single-units' histograms. J Neurosci Methods 5:317–325.

Carter RJ, Lione LA, Humby T, Mangiarini L, Mahal A, Bates GP, Dunnett SB, Morton AJ (1999) Characterization of progressive motor deficits in mice transgenic for the human Huntington's disease mutation. J Neurosci 19:3248–3257.

Cepeda C, Wu N, André VM, Cummings DM, Levine MS (2007) The corticostriatal pathway in Huntington's disease. Prog Neurobiol 81:253–271.

Cha JH, Kosinski CM, Kerner JA, Alsdorf SA, Mangiarini L, Davies SW, Penney JB, Bates GP, Young AB (1998) Altered brain neurotransmitter receptors in transgenic mice expressing a portion of an abnormal human Huntington disease gene. Proc Natl Acad Sci U S A 95:6480–6485.

Connors BW, Gutnick MJ (1990) Intrinsic firing patterns of diverse neocortical neurons. Trends Neurosci 13:99–104.

Contreras D (2004) Electrophysiological classes of neocortical neurons. Neural Netw 17:633–646.

Crawley JN, Belknap JK, Collins A, Crabbe JC, Frankel W, Henderson N, Hitzemann RJ, Maxson SC, Miner LL, Silva AJ, Wehner JM, Wynshaw-Boris A, Paylor R (1997) Behavioral phenotypes of inbred mouse strains: implications and recommendations for molecular studies. Psychopharmacology 132:107–124.

Crupi D, Ghilardi MF, Mosiello C, Di Rocco A, Quartarone A, Battaglia F (2008) Cortical and brainstem LTP-like plasticity in Huntington's disease. Brain Res Bull 75:107–114.

Cummings DM, Milnerwood AJ, Dallérac GM, Waights V, Brown JY, Vatsavayai SC, Hirst MC, Murphy KP (2006) Aberrant cortical synaptic plasticity and dopaminergic dysfunction in a mouse model of Huntington's disease. Hum Mol Genet 15:2856–2868.

Cummings DM, Milnerwood AJ, Dallérac GM, Vatsavayai SC, Hirst MC, Murphy KP (2007) Abnormal cortical synaptic plasticity in a mouse model of Huntington's disease. Brain Res Bull 72:103–107.

Cybulska-Klosowicz A, Mazarakis NK, Van Dellen A, Blakemore C, Hannan AJ, Kossut M (2004) Impaired learning-dependent cortical plasticity in Huntington's disease transgenic mice. Neurobiol Dis 17:427–434.

Dalley JW, Cardinal RN, Robbins TW (2004) Prefrontal executive and cognitive functions in rodents: neural and neurochemical substrates. Neurosci Biobehav Rev 28:771–784.

DiFiglia MM (1990) Excitotoxic injury of the neostriatum: a model for Huntington's disease. Trends Neurosci 13:286–289.

Dorner JL, Miller BR, Barton SJ, Brock TJ, Rebec GV (2007) Sex differences in behavior and striatal ascorbate release in the 140 CAG knock-in mouse model of Huntington's disease. Behav Brain Res 178:90–97.

Feigin A, Ghilardi M-F, Huang C, Ma Y, Carbon M, Guttman M, Paulsen JS, Ghez CP, Eidelberg D (2006) Preclinical Huntington's disease: compensatory brain responses during learning. Ann Neurol 59:53–59.

Fonnum F, Storm-Mathisen J, Divac I (1981) Biochemical evidence for glutamate as neurotransmitter in corticostriatal and corticothalamic fibres in rat brain. Neuroscience 6:863–873.

Gerstein GL (1999) Correlation-based analysis for neural ensemble data. In: Methods for neural ensemble recordings (Nicolelis MAL, ed), pp 157–177. Boca Raton, FL: CRC.

Gu X, Li C, Wei W, Lo V, Gong S, Li SH, Iwasato T, Itohara S, Li XJ, Mody I, Heintz N, Yang XW (2005) Pathological cell-cell interactions elicited by a neuropathogenic form of mutant Huntingtin contribute to cortical pathogenesis in HD mice. Neuron 46:433–444.

Hampson RE, Deadwyler SA (1999) Pitfalls and problems in the analysis of neuronal ensemble recordings during behavioral tasks. In: Methods for neural ensemble recordings (Nicolelis MAL, ed), pp 229–248. Boca Raton, FL: CRC.

Hestrin S, Galarreta M (2005) Electrical synapses define networks of neocortical GABAergic neurons. Trends Neurosci 28:304–309.

Hickey MA, Chesselet MF (2003) The use of transgenic and knock-in mice to study Huntington's disease. Cytogenet Genome Res 100:276–286.

Holmes A, Wrenn CC, Harris AP, Thayer KE, Crawley JN (2002) Behavioral profiles of inbred strains on novel olfactory, spatial and emotional tests for reference memory in mice. Genes Brain Behav 1:55–69.

Homayoun H, Moghaddam B (2007) NMDA receptor hypofunction produces opposite effects on prefrontal cortex interneurons and pyramidal neurons. J Neurosci 27:11496–11500.

Homayoun H, Jackson ME, Moghaddam B (2005) Activation of metabotropic glutamate 2/3 receptors reverses the effects of NMDA receptor hypofunction on prefrontal cortex unit activity in awake rats. J Neurophysiol 93:1989–2001.

Izhikevich EM, Desai NS, Walcott EC, Hoppensteadt FC (2003) Bursts as a unit of neural information: selective communication via resonance. Trends Neurosci 26:161–167.

Jackson ME, Homayoun H, Moghaddam B (2004) NMDA receptor hypofunction produces concomitant firing rate potentiation and burst activity reduction in the prefrontal cortex. Proc Natl Acad Sci U S A 101:8467–8472.

Jung MW, Qin Y, McNaughton BL, Barnes CA (1998) Firing characteristics of deep layer neurons in prefrontal cortex in rats performing spatial working memory tasks. Cereb Cortex 8:437–450.

Kemp JM, Powell TP (1971) The termination of fibres from the cerebral cortex and thalamus upon dendritic spines in the caudate nucleus: a study with the Golgi method. Philos Trans R Soc Lond B Biol Sci 262:429–439.

Laforet GA, Sapp E, Chase K, McIntyre C, Boyce FM, Campbell M, Cadigan BA, Warzecki L, Tagle DA, Reddy PH, Cepeda C, Calvert CR, Jokel ES, Klapstein GJ, Ariano MA, Levine MS, DiFiglia M, Aronin N (2001) Changes in cortical and striatal neurons predict behavioral and electrophysiological abnormalities in a transgenic murine model of Huntington's disease. J Neurosci 21:9112–9123.

Lange H, Thörner G, Hopf A, Schröder KF (1976) Morphometric studies of the neuropathological changes in choreatic diseases. J Neurol Sci 28:401–425.

Lawrence AD, Sahakian BJ, Hodges JR, Rosser AE, Lange KW, Robbins TW (1996) Executive and mnemonic functions in early Huntington's disease. Brain 119:1633–1645.

Lawrence AD, Sahakian BJ, Robbins TW (1998) Cognitive functions and corticostriatal circuits: insights from Huntington's disease. Trends Cogn Sci 2:379–388.

Legéndy CR, Salcman M (1985) Bursts and recurrences of bursts in the spike trains of spontaneously active striate cortex neurons. J Neurophysiol 53:926–939.

Lewicki MS (1998) A review of methods for spike sorting: the detection and classification of neural action potentials. Network 9:R53–R78.

Liévens JC, Woodman B, Mahal A, Spasic-Boscovic O, Samuel D, Kerkerian-Le Goff L, Bates GP (2001) Impaired glutamate uptake in the R6 Huntington's disease transgenic mice. Neurobiol Dis 8:807–821.

Lione LA, Carter RJ, Hunt MJ, Bates GP, Morton AJ, Dunnett SB (1999) Selective discrimination learning impairments in mice expressing the human Huntington's disease mutation. J Neurosci 19:10428–10437.

Lisman JE (1997) Bursts as a unit of neural information: making unreliable synapses reliable. Trends Neurosci 20:38–43.

Mangiarini L, Sathasivam K, Seller M, Cozens B, Harper A, Hetherington C, Lawton M, Trottier Y, Lehrach H, Davies SW, Bates GP (1996) Exon 1 of the HD gene with an expanded CAG repeat is sufficient to cause a progressive neurological phenotype in transgenic mice. Cell 87:493–506.

Mazarakis NK, Cybulska-Klosowicz A, Grote H, Pang T, Van Dellen A, Kossut M, Blakemore C, Hannan AJ (2005) Deficits in experience-dependent cortical plasticity and sensory-discrimination learning in presymptomatic Huntington's disease mice. J Neurosci 25:3059–3066.

McCormick DA, Connors BW, Lighthall JW, Prince DA (1985) Comparative electrophysiology of pyramidal and sparsely spiny stellate neurons of the neocortex. J Neurophysiol 54:782–806.

Menalled LB (2005) Knock-in mouse models of Huntington's disease. NeuroRx 2:465–470.

Menalled LB, Sison JD, Dragatsis I, Zeitlin S, Chesselet MF (2003) Time course of early motor and neuropathological anomalies in a knock-in mouse model of Huntington's disease with 140 CAG repeats. J Comp Neurol 465:11–26.

Miller BR, Dorner JL, Shou M, Sari Y, Barton SJ, Sengelaub DR, Kennedy RT, Rebec GV (2008a) Up-regulation of GLT1 expression increases glutamate uptake and attenuates the Huntington's disease phenotype in the R6/2 mouse. Neuroscience 153:329–337.

Miller BR, Walker AG, Shah AS, Barton SJ, Rebec GV (2008b) Dysregulated information processing by medium-spiny neurons in striatum of freely behaving mouse models of Huntington's disease. J Neurophysiol, in press.

Morton AJ, Wood NI, Hastings MH, Hurelbrink C, Barker RA, Maywood ES (2005) Disintegration of the sleep-wake cycle and circadian timing in Huntington's disease. J Neurosci 25:157–163.

Murphy KP, Carter RJ, Lione LA, Mangiarini L, Mahal A, Bates GP, Dunnett SB, Morton AJ (2000) Abnormal synaptic plasticity and impaired spatial cognition in mice transgenic for exon 1 of the human Huntington's disease mutation. J Neurosci 20:5115–5123.

Nguyen PV (2006) Comparative plasticity of brain synapses in inbred mouse strains. J Exp Biol 209:2293–2303.

Paulsen JS, Zimbelman JL, Hinton SC, Langbehn DR, Leveroni CL, Benjamin ML, Reynolds NC, Rao SM (2004) fMRI biomarker of early neuronal dysfunction in presymptomatic Huntington's disease. Am J Neuroradiol 25:1715–1721.

Paxinos G, Franklin K (2001) The mouse brain in stereotaxic coordinates, Ed 2. San Diego: Academic.

Perkel DH, Gerstein GL, Moore GP (1967) Neuronal spike trains and stochastic point processes. II. Simultaneous spike trains. Biophys J 7:419–440.

Rebec GV, Barton SJ, Ennis MD (2002) Dysregulation of ascorbate release in the striatum of behaving mice expressing the Huntington's disease gene. J Neurosci 22:RC202(1–5).

Rebec GV, Barton SJ, Marseilles AM, Collins K (2003) Ascorbate treatment attenuates the Huntington behavioral phenotype in mice. Neuroreport 14:1263–1265.

Rebec GV, Conroy SK, Barton SJ (2006) Hyperactive striatal neurons in symptomatic Huntington R6/2 mice: variations with behavioral state and repeated ascorbate treatment. Neuroscience 137:327–336.

Sakurai Y (1999) How do cell assemblies encode information in the brain? Neurosci Biobehav Rev 23:785–796.

Sakurai Y, Takahashi S (2006) Dynamic synchrony of firing in the monkey prefrontal cortex during working-memory tasks. J Neurosci 26:10141–10153.

Schiefer J, Sprünken A, Puls C, Lüesse HG, Milkereit A, Milkereit E, Johann V, Kosinski CM (2004) The metabotropic glutamate receptor 5 antagonist MPEP and the mGluR2 agonist LY379268 modify disease progression in a transgenic mouse model of Huntington's disease. Brain Res 1019:246–254.

Schoepp DD, Jane DE, Monn JA (1999) Pharmacological agents acting at subtypes of metabotropic glutamate receptors. Neuropharmacology 38:1431–1476.

Sesack SR, Deutch AY, Roth RH, Bunney BS (1989) Topographical organization of the efferent projections of the medial prefrontal cortex in the rat: an anterograde tract-tracing study with *Phaseolus vulgaris* leucoagglutinin. J Comp Neurol 290:213–242.

Sotrel A, Williams RS, Kaufmann WE, Myers RH (1993) Evidence for neuronal degeneration and dendritic plasticity in cortical pyramidal neurons of Huntington's disease: a quantitative Golgi study. Neurology 43:2088–2096.

The Huntington's Disease Collaborative Research Group (1993) A novel gene containing a trinucleotide repeat that is expanded and unstable on Huntington's disease chromosomes. Cell 72:971–983.

Thiruvady DR, Georgiou-Karistianis N, Egan GF, Ray S, Sritharan A, Farrow M, Churchyard A, Chua P, Bradshaw JL, Brawn TL, Cunnington R (2007) Functional connectivity of the prefrontal cortex in Huntington's disease. J Neurol Neurosurg Psychiatry 78:127–133.

Vertes RP (2004) Differential projections of the infralimbic and prelimbic cortex in the rat. Synapse 51:32–58.

Vonsattel JP, Myers RH, Stevens TJ, Ferrante RJ, Bird ED, Richardson EP Jr (1985) Neuropathological classification of Huntington's disease. J Neuropathol Exp Neurol 44:559–577.

Wilson CJ, Kawaguchi Y (1996) The origins of two-state spontaneous membrane potential fluctuations of neostriatal spiny neurons. J Neurosci 16:2397–2410.

Young ED, Robert JM, Shofner WP (1988) Regularity and latency of units in ventral cochlear nucleus: implications for unit classification and generation of response properties. J Neurophysiol 60:1–29.

Zar JH (1999) Biostatistical analysis, Ed 4. Upper Saddle River, NJ: Prentice Hall.